Acta Materialia. Vol. 53. Núm. 4. 2005. Pag. 1241-1251
http://dx.doi.org/10.1016/j.actamat.2004.11.018

Partial Substitution of Co and Ge for Fe and B in Fe-Zr-B-Cu Alloys: Microstructure and Soft Magnetic Applicability at High Temperature.

J. S. Blázquez,[1,2] S. Roth,[1] C. Mickel,[1] A. Conde [2]

[1] *IFW-Dresden, Institute for Metallic Materials, Helmholtzstrasse 20, 01069 Dresden, Germany.*

[2] *Departamento de Física de la Materia Condensada. ICMSE-CSIC. Universidad de Sevilla. P.O. Box 1065. 41080 Sevilla, Spain.*

Keywords: nanocrystalline microstructure, soft magnets, HITPERM alloys.

PACS: 61.46.+w; 75.50.Tt; 75.75+a.

Abstract

The partial substitutions of Co for Fe and Ge for B are studied for a $Fe_{83-x}Co_xZr_6B_{10-y}Ge_yCu_1$ alloy series (x = 0, 5 and 20; y = 0 and 5) as a possible way to enhance the high temperature applicability of NANOPERM alloys. The devitrification process, the nanocrystallization kinetics and the nanocrystalline microstructure are similar for all the studied alloys. Good soft magnetic properties are observed even at a high crystalline volume fraction of bcc α-Fe nanocrystals, which are stable up to ~1000 K. The partial substitution of Co for Fe is very effective to increase the Curie temperature of the residual amorphous matrix (T_C^{AM}). Although the substitution of Ge for B is ineffective to increase T_C^{AM}, a clear increase of the saturation magnetization with respect to the Ge-free alloy can be observed.

**Corresponding author*: Dr. Javier S. Blázquez

IFW Dresden Institute for Metallic Materials

P.O. Box 27 00 16, D-01171 Dresden, GERMANY

Tel. +49 351 4659 253

Fax +49 351 4659 541

Acta Materialia. Vol. 53. Núm. 4. 2005. Pag. 1241-1251
http://dx.doi.org/10.1016/j.actamat.2004.11.018

1. Introduction

Nanocrystalline Fe-based alloys exhibit outstanding soft magnetic properties characterized by a very low coercivity and a very high saturation magnetization [1]. These alloys have a microstructure in which nanocrystals of a ferromagnetic α-Fe type phase (~10 nm in size) are embedded in a residual amorphous matrix, also ferromagnetic but with a lower Curie temperature. The ferromagnetic character of this matrix enables the exchange coupling between nanocrystals, which yield a severe reduction of the average magnetocrystalline anisotropy [2,3].

These nanocrystalline compositions have a high concentration of Fe and a typical composition: Fe-M-ET-(Cu), where M is a metalloid and ET is an early transition metal. The addition of metalloids, such as B, P, Si, etc., is necessary to enable the production of a precursor amorphous alloy by rapid quenching techniques, from which the nanocrystalline microstructure is obtained after controlled crystallization. It is important to distinguish two different kinds of metalloids: those highly soluble in the α-Fe phase (e.g. Si) and those whose solubility in this phase is very restricted (e.g. B). The former elements will be generally dissolved in the crystalline phase, increasing the crystalline volume fraction but deteriorating some magnetic properties like the saturation magnetization and the Curie temperature of the crystalline phase. The latter elements will remain in the amorphous matrix and will diminish the maximum volume fraction of nanocrystals, although preserving the purity of the α-Fe phase.

The early transition metals (Zr, Nb, Hf, etc.) have a very low solubility in the α-Fe phase and, consequently, will remain in the amorphous matrix. However, due to the very slow diffusivity of these elements in the amorphous phase, they pile up at the crystal-matrix interface and constrain the growth of the crystalline phase to the nanocrystalline scale.

The addition of Cu is not necessary to obtain the nanocrystalline microstructure in some compositions named NANOPERM [4] but, generally, enhances the soft magnetic

Acta Materialia. Vol. 53. Núm. 4. 2005. Pag. 1241-1251
http://dx.doi.org/10.1016/j.actamat.2004.11.018

properties of the material by refining the microstructure [5] through the formation of Cu-rich clusters previous to the nanocrystallization.

The original compositions have been slightly modified by the addition of other elements, in order to achieve specific characteristics for different applications [1]. In particular, since the production of HITPERM alloys by Willard et al. in 1998 [6], the extension of the applicability of nanocrystalline alloys to higher temperatures is becoming an intensive area of research in the recent years. This alloy, of composition $Fe_{44}Co_{44}Zr_7B_4Cu_1$, was proposed mainly because of the strong increase of the Curie temperature of the residual amorphous phase (T_C^{AM}) due to the partial substitution of Co for Fe with respect to the Co-free NANOPERM alloy [7]. In fact, the exchange coupling between nanocrystals is transmitted through the ferromagnetic residual amorphous matrix and thus, at temperatures above the Curie temperature of this residual amorphous matrix, the nanocrystals become exchange uncoupled and, consequently, the outstanding soft magnetic properties of these nanocrystalline alloys are lost [3].

Although a high saturation magnetization was achieved in HITPERM alloys [6], as well as a wide temperature range of constant permeability [8], the coercivity at room temperature increases one or two orders of magnitude with respect to the Co-free alloys (from 1-10 A/m up to ~100 A/m [6,9]). Focusing on this problem, Suzuki et al. recently proposed a small substitution of Ge for Fe as a more effective way to improve soft magnetic properties at high temperatures than the partial substitution of Co for Fe [10]. However, it must be taken into account that the substitution of Fe by a “non-magnetic” atom will provoke a reduction of the magnetization of the material. On the other hand, Cremaschi et al. found a reduction of the coercivity in FINEMET-type alloys after the substitution of Ge for B [11].

In this work, the combined effect of partial substitution of Co for Fe and Ge for B on the microstructure and the magnetic properties of nanocrystalline alloys is studied. The maximum Co concentration studied in the alloys is 20 at. %, in order to search for a new

Acta Materialia. Vol. 53. Núm. 4. 2005. Pag. 1241-1251
http://dx.doi.org/10.1016/j.actamat.2004.11.018

composition with competitive values of coercivity at room temperature, since previous studies showed that this parameter is seriously deteriorated for higher Co contents [6-9]. Although Ge is soluble in α-Fe, the benefits of its addition to NANOPERM alloys would be due to its partition to the residual amorphous matrix [10], not producing a deleterious effect on the crystalline phase. In this work, the role of Ge is also studied as the Co content increases in the alloy.

2. Experimental

Ribbons (~5 mm wide and 20-30 μm thick) of $Fe_{83}Zr_6B_{10}Cu_1$, $Fe_{78}Co_5Zr_6B_{10}Cu_1$, $Fe_{78}Co_5Zr_6Ge_5B_5Cu_1$ and $Fe_{63}Co_{20}Zr_6Ge_5B_5Cu_1$ were obtained in amorphous structure by melt-spinning. For simplicity, they will be referred in the following only by their Co and Ge concentration: *Co0Ge0*, *Co5Ge0*, *Co5Ge5* and *Co20Ge5* alloys, respectively. The devitrification and melting process of the as-cast ribbons were studied by differential scanning calorimetry (DSC) using a Perkin-Elmer DSC7 calorimeter for temperatures below 973 K and a Netzsch DSC-404C calorimeter for temperatures up to 1623 K. In order to study the dependence of magnetic properties on the microstructure, as-cast samples were heated up to different selected temperatures at 10 K/min, using the calorimeter, and immediately cooled down to room temperature at the maximum available rate (≥ 100 K/min). Both heating and cooling processes were performed in an argon flow. The microstructure of these samples was characterized by X-ray diffraction (XRD) using Co-Kα radiation (λ=0.178897 nm) in a Philips PW1050 diffractometer and by Transmission Electron Microscopy (TEM) using a JEOL 2000 FX operated at 200 kV. Saturation magnetization (M_S) as a function of temperature and Curie temperature (T_C) were studied using a Faraday magnetometer. Coercivity (H_C) was measured using a Förster Koerzimat. The saturation magnetostriction constant, λ_S, of as-cast samples was measured applying the small angle magnetization rotation method (SAMR) [12] on long samples (~5 mm wide and ~150 mm long).

Acta Materialia. Vol. 53. Núm. 4. 2005. Pag. 1241-1251
http://dx.doi.org/10.1016/j.actamat.2004.11.018

3. Results and discussion

3.1 Calorimetry

Figure 1 shows the DSC scans performed at 20 K/min for the four alloys in the temperature range corresponding to the crystallization phenomena. All the alloys present a similar devitrification process with two main exothermic peaks. The onset of the first transformation stage increases in the sense: *Co20Ge5* < *Co5Ge5* < *Co5Ge0* < *Co0Ge0*. Therefore, it is evidenced that a substitution of Co for Fe decreases the thermal stability of the initial amorphous alloy, as it was found for other nanocrystalline systems [6,7,13]. On the other hand, substitution of Ge for B also decreases the stability of the amorphous alloy, although the partial substitution of Ge for Fe was reported as not affecting the crystallization onset temperature [10]. The measurement of the enthalpy of transformation is strongly affected by the selection of the baseline, especially for wide DSC peaks. However, once the same criteria have been assumed, the enthalpy of the first transformation stage is always clearly larger for the *Co20Ge5* alloy than for the other three alloys. Different studies on Fe-Co based nanocrystalline alloys show that the Co concentration is neither enriched nor depleted in the α-Fe phase and the nanocrystals are enriched only in Fe [14-16]. The observed changes in the enthalpy of the first transformation stage of these alloys can be related to that fact because, as the Fe content of the alloy decreases, a larger volume of the material will be affected during the growth of a nanocystal up to certain diameter. A very simple picture will be helpful to understand this assertion. In this picture, a spherical nanocrystal of 10 nm in size is surrounded by other sphere, which would supply all the Fe needed to enrich the nanocrystal. Therefore, at the initial state, the concentration of the whole system is that of the as-cast amorphous. After the nanocrystallization, inside the smaller sphere (nanocrystal) the Fe content is enriched up to fulfill the atomic percent which previously corresponded to the other elements different than Fe and Co (17 at. % in the studied cases) and outside the smaller

Acta Materialia. Vol. 53. Núm. 4. 2005. Pag. 1241-1251
http://dx.doi.org/10.1016/j.actamat.2004.11.018

sphere the concentration of Fe is 0. A simple balance between the initial and the final state will supply the volume of the larger sphere, which is related with the affected volume during the nanocrystallization of a nanocrystal of 10 nm in diameter. This volume continuously increases with the decrease of the Fe content in the alloy, being 1205, 1218 and 1270 nm^3 for the alloys with 0, 5 and 20 at. % of Co, respectively. In this picture, it has been assumed very abrupt and unrealistic concentration profiles of Fe, but the increase of the volume affected during the formation of a single nanocrystal, as the Fe content in the alloy decreases, can be extrapolated to a more realistic picture in which the concentration profiles will be smeared. Therefore, a larger volume affected should provoke a larger enthalpy associated with the development of the nanocrystalline microstructure with the same crystalline volume fraction, as it has been observed in the studied system and for other HITPERM alloy series [13]. Table I summarizes the main parameters obtained from the calorimetric studies.

The kinetics of the first transformation, corresponding to the development of the nanocrystalline microstructure, was studied by three different non-isothermal approaches: Kissinger [17], Augis-Bennett [18] and Gao-Wang [19] methods. A set of four scans obtained at heating rates of 5, 10, 20 and 40 K/min was used for each alloy. Although the Kissinger method is the most widely used, its theoretical validity for describing crystallization of amorphous metals has been questioned by some authors [20,21]. The Kissinger method can be summarized in the following expression:

$$\frac{d\left(Ln\left[\beta / T_p^{\,2}\right]\right)}{d\left(1/T_p\right)} = -\frac{Q}{R} \tag{1}$$

where β is the heating rate, T_p the peak temperature (considered as the temperature at which the transformation rate is maximum), Q is the activation energy and R is the gas constant.

On the other hand, the Augis-Bennett method considers the influence of the onset temperature, T_X, and yields the expression:

Acta Materialia. Vol. 53. Núm. 4. 2005. Pag. 1241-1251
http://dx.doi.org/10.1016/j.actamat.2004.11.018

$$\frac{d\left(Ln\left[\beta/\left(T_p - T_X\right)\right]\right)}{d\left(1/T_p\right)} = -\frac{Q}{R} \tag{2}$$

Finally, the Gao-Wang method supplies two expressions for calculating Q and the Avrami exponent, n, respectively:

$$\frac{d\left(Ln\left[\left(dX/dt\right)_p\right]\right)}{d\left(1/T_p\right)} = -\frac{Q}{R} \tag{3}$$

and

$$(dX/dt)_p = 0.37n\beta Q/(RT_p^2) \tag{4}$$

where $(dX/dt)_p$ is the transformation rate at the peak temperature.

The kinetic parameters are listed in table II. The values of Q obtained by the three different methods are consistent, although the values obtained by the Kissinger method are always lower than those obtained by the Gao-Wang method and these are lower than those obtained by the Augis-Bennett method. The *Co20Ge5* alloy shows the lowest value of Q (~3 eV) and the *Co0Ge0* alloy presents the highest value of Q (~4 eV), confirming the decrease of the thermal stability of the amorphous phase as Co and Ge are substituted for Fe and B, respectively. These values are similar to those found for NANOPERM and HITPERM alloys [1,22-24]. The value of the Avrami exponent of the nanocrystallization process is close to 1 for all the studied alloys. This value is characteristic for the kinetics of the nanocrystallization of metallic amorphous alloys [1,22,23].

The shape of the peak of the second transformation stage is clearly asymmetric for the alloys with Ge (much clearer for the alloy with 20 at. % of Co), while it is sharp and symmetric for the alloys without Ge. The enthalpy involved in the process is comparable in all the studied cases, ~37 J/g. The peak temperature of the second crystallization process increases in the sense *Co5Ge0* < *Co20Ge5* ~ *Co0Ge0* < *Co5Ge5* alloy. However, if the onset of the second crystallization stage is used, the strong asymmetry of this peak in the alloys with

Ge alters this order being *Co20Ge5* < *Co5Ge5* < *Co5Ge0* ~ *Co0Ge0*, where a difference has been considered significant if it is larger than 3 K.

Between the second transformation stage and the melting of the system detected by calorimetry, there are no clear events, except for an endothermic process at ~1225 K detected for the *Co20Ge5* alloy, which corresponds to the α-γ transition of the Fe(Co) crystalline phase. A similar feature, although much weaker and at higher temperatures, is detected for the *Co0Ge0* (~1250 K) and *Co5Ge0* (~ 1240 K) alloys. In the case of the *Co5Ge5* alloy, no remarkable endothermic process is detected. This can be due to the presence of Ge within the nanocrystals. In fact, the α-γ transition is totally avoided for a Ge content > 4 at. % [25]. The temperature value of the endotherm detected for the *Co20Ge5* alloy is in agreement with a content of ~20 at. % of Co in the Fe(Co) phase [25]. As it will be discussed in more detail below, the decrease of the lattice parameter of the α-Fe(Co) phase, observed for *Co20Ge5* alloy after the second crystallization stage, also supports the idea of a rejection of Ge from the α-Fe(Co) to other intermetallics. However, for the other two alloys, without Ge, the shift of the endothermic peak to higher temperatures cannot be understood in terms of Co or Ge effects. As it will be shown later in this paper, XRD patterns of fully crystallized samples show that the main phase at room temperature is α-Fe in all the studied cases, thus the α-γ transition might be the candidate for this endotherm. A possible slow recrystallization of the α-Fe phase corresponding to broad peaks at temperatures higher than 1000 K and which are weak enough to prevent their detection by DSC could be another possible explanation of the absence of a clear α-γ transition in these Ge-free alloys.

The melting behavior of the alloys can be divided in two different groups: the alloys with Ge present a clear two-peaks structure, meanwhile the alloys without Ge show a strong single peak preceded by a tiny feature at about 1500-1550 K. The onset of the melting

increases in the same sense as the onset of the nanocrystallization does: *Co20Ge5* < *Co5Ge5* < *Co5Ge0* < *Co0Ge0* (see Table I).

3.2 Microstructure

As-cast samples of the different alloys were heated at 10 K/min up to different temperatures, T_A, in the range from 573 to 1073 K, and immediately cooled down, in order to study the evolution of the microstructure along the crystallization process. At low T_A, only the amorphous halo is detected. The diffraction maxima corresponding to the α-Fe type phase appear for samples heated above 782, 782, 757 and 732 K for the *Co0Ge0*, *Co5Ge0*, *Co5Ge5* and *Co20Ge5* alloys, respectively, in agreement with the observed onsets of the first crystallization stage. During this process, a nanocrystalline microstructure develops as a two-phase system consisting of α-Fe type nanocrystals embedded in a residual amorphous matrix. As T_A increases, the diffraction maxima of the crystalline phase increase and the intensity of the amorphous halo decreases. After annealing at temperatures above 923-973 K, the amorphous halo disappears and new crystalline peaks appear.

For the nanocrystalline samples, a deconvolution procedure was applied to the (110) maximum and the amorphous halo in order to extract more information from the XRD patterns. A Lorentzian function was used to fit the crystalline peak, assuming that the small crystalline size is the main reason for the broadening of the diffraction maximum. The amorphous halo was fitted using a Gaussian function. After this deconvolution process, the evolution of both residual amorphous and crystalline α-Fe type phases could be studied in detail.

3.2.1 Amorphous phase.

The as-cast samples are fully amorphous. This phase coexists with the nanocrystals of α-Fe along the first transformation process. The volume fraction of this phase, calculated

Acta Materialia. Vol. 53. Núm. 4. 2005. Pag. 1241-1251
http://dx.doi.org/10.1016/j.actamat.2004.11.018

from the area ratio between the amorphous halo and the (110) maximum, decreases down to 20-15 % at the end of the nanocrystallization process. After the second crystallization stage, the amorphous phase disappears and other intermetallic phases form. The parameters obtained from the deconvolution procedure described above and characterizing the amorphous halo are: the area, the central position and the full width at half maximum of the halo.

The area was used to calculate the crystalline volume fraction of the nanocrystals. The width of the amorphous halo is ~10 degrees and the simplicity of our fitting model prevents a further discussion about this parameter. However, a clear evolution in the position of the amorphous halo is observed as T_A increases, as it can be seen in figure 2a. For fully amorphous samples, the position of the halo is almost constant. However, the amorphous halo clearly shifts to lower values of 2θ as the nanocrystallization progresses.

The position of the amorphous halo can be associated with the interatomic distance between neighboring atoms as [26]:

$$\delta = \frac{5\lambda}{8\sin(\theta)} \qquad (5)$$

where λ is the wavelength of the X-rays used, 0.178897 nm.

Therefore, a continuous shift of the halo to lower values of 2θ implies a continuous increase of the average interatomic distance in the amorphous phase. On the other hand, using the Goldschmidt atomic radii of the different elements [27], it is possible to calculate a theoretical distance between the atoms of the residual amorphous phase as the average diameter of the atoms in this phase. In order to do so, it is necessary to know the composition of the residual amorphous matrix and its dependence on the crystalline volume fraction. A general formula to calculate the concentration of the different elements in the residual amorphous phase would be:

$$C_{RA} = \frac{C_{IA} - C_{CR}X}{1 - X} \qquad (6)$$

Acta Materialia. Vol. 53. Núm. 4. 2005. Pag. 1241-1251
http://dx.doi.org/10.1016/j.actamat.2004.11.018

where C_{IA}, C_{RA} and C_{CR} indicate the concentration in the initial amorphous, the residual amorphous and the crystalline phases, respectively, and X is the crystalline volume fraction.

The α-Fe crystalline phase formed in the *Co0Ge0* alloy is expected to be close to pure Fe, due to the low solubility of the rest of the elements in this lattice. This fact largely simplifies the calculations, being C_{CR} = 100 for Fe and 0 for the other elements. Therefore, the following discussion will be referred to the *Co0Ge0* alloy, the amorphous matrix of which is enriched in B and Zr and impoverished in Fe as the nanocrystallization progresses.

Once the composition of the residual amorphous matrix has been calculated for every value of X, it is straightforward to calculate the average distance between atoms using Goldschmidt atomic radii. If B atoms were taken into account, the average distance between atoms would continuously decrease due to the strong enrichment in B of the amorphous matrix, differing from the experimental result. However, the observed trend is reproduced if the contribution of the B atoms to the amorphous halo profile is neglected. This light element has the lowest scattering factor of all the elements in the alloy (For $\sin\theta/\lambda \sim 2.4$ nm^{-1}, since $2\theta \sim 50°$ and $\lambda \sim 0.178897$ nm, the atomic scattering factors are ~2 for B, ~20 for Fe, Co, Ge and Cu, and ~30 for Zr [28]). For this reason, only the metallic atoms will be taken into account, considering B in interstitials-like positions, and the enrichment of the amorphous matrix in Zr as the nanocrystallization progresses would yield an increase of the distance between metallic atoms. Figure 2b shows the evolution of the experimental distance calculated from the position of the amorphous halo for the *Co0Ge0* alloy. The average values of the interatomic distance calculated in both cases, when B atoms are considered or neglected, are also shown. Although the approximation is quite vague, it would be worthy to note that the consideration of B atoms would yield a continuous shift of the amorphous halo position to higher 2θ values, in contradiction with the observed experimental trend. Therefore, it might be inferred that the amorphous halo position mainly depends on the distances between metallic atoms without considering the distance between B atoms and their nearest

neighbors. For the other three alloys, after assuming a constant composition for the α-Fe(Co,Ge) phase, which allows the use of expression (6), it is also observed that the agreement is better if B atoms are not considered to contribute to the amorphous halo position.

3.2.2 Nanocrystals

As it was said above, the area ratio between the (110) maximum and the amorphous halo was used to obtain the crystalline volume fraction, *X*, for the nanocrystalline state. The lattice parameter of the α-Fe type phase, *a*, was obtained from the position of the (110) and the (200) maxima and the average grain size, $<D>$, was calculated from the broadening of the (110) maximum using the Scherrer formula. Figure 3 shows the evolution of the crystalline volume fraction against the difference between the treatment temperature and the crystallization onset temperature (T_A-T_X) and figure 4 shows the grain size and the lattice parameter against *X* for the annealed samples of the four studied alloys.

The nanocrystalline microstructures developed in the alloys are very similar. Both *X* and $<D>$ increase monotonously, the former up to a saturation value of about 80-85 % and the latter up to ~10 nm at the end of the nanocrystallization process. From these two parameters, the number density of nanocrystals, N_V, can be obtained as:

$$N_V = \frac{6X}{\pi < D >^3} \qquad (7)$$

For values of the crystalline volume fraction higher than 30 %, this value is almost constant considering the error bars, ~$2*10^{-3}$ nm^{-3}. This implies that the nucleation process is limited to the early stages of the nanocrystallization.

The lattice parameter of the α-Fe phase shows a continuous decrease as the nanocrystallization progresses, independent on the composition of the alloy. In fact, this cannot be associated only with compositional changes of the crystallites during the

nanocrystallization. For example, in the *Co0Ge0* alloy, the expected composition is 100 % Fe, since Zr and B have such low solubility in α-Fe that they are expected to be rejected from the crystalline phase completely. For this alloy, a continuous increase of the grain size is observed as the crystalline volume fraction increases. On the other hand, there are studies indicating a dilatation of the unit cell in nanocrystalline systems with respect to the equilibrium value due to the small size of the crystallites. Zhao et al. [29] reported that the unit cell volume increases in nanocrystalline Se with respect to the microcrystalline value. It is established in that paper that the ratio between the nanocrystalline unit cell volume and that of the microcrystalline system ranges from 1.001 to 1.007 as the grain size reduces from 70 to 13 nm [29]. Therefore, this effect might be also considered to contribute to the observed decrease of the lattice parameter in our alloys. On the other hand, the two alloys with Ge show higher values of *a* than those observed for the alloys without Ge. This could be due to the presence of Ge within the nanocrystal, because Co has no effect on the lattice parameter of α-Fe below 20 at. % and a higher content even yields a reduction of *a* [30]. The maximum solubility of Ge in α-Fe, ~10 at. % [25], allows the presence of Ge inside the nanocrystals. The lattice parameter of α-Fe increases by ~1.7 10^{-13} m per at. % of Ge [31], which implies a shift in the 2θ value of the diffraction maxima of the α-Fe type phase obtained with Co-Kα radiation of about 0.03 and 0.06 degrees per at. % of Ge for the (110) and (200), respectively. These values are of the order of the step scan of the data acquisition program (0.05 degrees) and therefore, it must be considered as a limit to the sensitivity of the experiment. Therefore, the difference observed at the end of the nanocrystallization can be explained by a Ge content of about 2 at. % for the *Co5Ge5* alloy and of about 4-5 at. % for the *Co20Ge5* alloy. These values, although lower than the nominal concentration of Ge in the as-cast alloy, should indicate a worsening of the preferential partitioning of Ge to the amorphous matrix as the Co content increases in the alloy. The tendency of Ge to enrich in the amorphous matrix was explained in terms of the

lower heat of mixing between Ge and Zr (-60 kJ/mol) [32] compared to that between Ge and Fe (-3 kJ/mol) [32], which provokes that Ge will follow the rejected Zr atoms from the crystalline phase to the matrix [10,33]. However, the heat of mixing between Ge and Co (-9 kJ/mol) [32] is slightly more negative than that between Fe and Ge and, consequently, could affect the partitioning behavior of Ge in the nanocrystalline state.

The microstructure of the nanocrystallized samples was also studied by TEM. Figure 5 shows the bright field images as well as the selected area diffraction pattern (inset) for samples of *Co5Ge5* and *Co20Ge5* alloys annealed at 873 K. As it can be observed, this technique confirms the microstructure derived from XRD data. Both compositions exhibit a similar microstructure in which nanocrystals of α-Fe type phase, of about 10 nm diameter, are embedded in a residual amorphous matrix.

3.2.3 High temperature phases

Figure 6 shows the XRD patterns of the four alloys heated up to 1073 K, beyond the completion of the second transformation stage. The main peaks appearing in each pattern correspond to the α-Fe phase. In order to have an idea of the evolution of the α-Fe(Co,Ge) phase after the second crystallization process, the area of the (110) maximum was compared to the full area of the pattern ranging from 30 to 70 degrees of 2θ. This calculation showed that the area ratio between the (110) maximum and the whole range (which for nanocrystalline samples was approached to the crystalline volume fraction) slightly decreases for the *Co0Ge0* alloy (from ~0.8 to ~0.75), although for the other alloys the decrease is more evident (down to ~0.65). This indicates a stronger tendency to the recrystallization of the α-Fe phase when there is some Co dissolved in it, involving a reaction of the amorphous matrix with some of the nanocrystals to form other crystalline phases. In fact, previous studies showed that a recrystallization process occurs during the second crystallization stage of Fe-Co-Nb-B-Cu alloys, which is enhanced as the Co content increases in the alloy [34].

Acta Materialia. Vol. 53. Núm. 4. 2005. Pag. 1241-1251
http://dx.doi.org/10.1016/j.actamat.2004.11.018

In the case of the *Co0Ge0*, *Co5Ge0* and *Co5Ge5* alloys, the lattice parameter of the α-Fe phase of fully crystallized samples does not significantly change with respect to the samples annealed at the end of the nanocrystallization. However, a clear decrease of *a* was observed in fully nanocrystallized samples of *Co20Ge5* alloy (0.2865 nm) with respect to the value of *a* at the end of the nanocrystallization process (0.2872 nm). As it was pointed above in the *Calorimetry* section, this decrease should indicate a rejection of Ge from the α-Fe(Co) phase to new intermetallic phases such as $Fe_{23}Zr_6$, only detected for the *Co20Ge5* alloy after the second crystallization stage. The rejection of Ge from the α-Fe(Co) crystals would assure the presence of the allotropic α-γ transition, clearly observed for this alloy by DSC techniques as an endothermic peak at ~1225 K (see fig. 1), which is suppressed for a Ge content higher than 4 at. % [25].

The simplest XRD patterns after fully crystallization are those of the Ge-free alloys. However, the observed peaks cannot be unambiguously indexed. Although a possible candidate would be the Fe_2Zr phase, it must be taken into account that the B content of the residual amorphous matrix at the end of the nanocrystallization is as high as 50 at. % and, therefore, a metastable B containing phase could be the responsible for the diffraction maxima.

The alloys with Ge show an extra diffraction maximum at ~42 degrees. Nevertheless, no Ge containing phase was found exhibiting any strong maximum around this value. This peak could correspond to a Zr rich phase, even α-Zr phase. The lower B content of these alloys with respect to the Ge-free alloys could be responsible for the formation of this Zr rich phase. For Ge-free alloys, the ratio between B and Zr content is 10/6 in at. %, whereas this ratio decreases down to 5/6 in Ge-containing alloys. The amount of B in the residual amorphous matrix could not be large enough to absorb all the Zr atoms and therefore these atoms may form another phase. In the case of the *Co20Ge5* alloy, new peaks appear with

Acta Materialia. Vol. 53. Núm. 4. 2005. Pag. 1241-1251
http://dx.doi.org/10.1016/j.actamat.2004.11.018

respect to the XRD pattern of the *Co5Ge5* alloy, which can be associated to a $Fe_{23}Zr_6$ type phase.

3.3 Magnetic properties

3.3.1 Curie temperature.

Figure 7 shows the evolution of the saturation magnetization, M_S, with the temperature for as-cast samples of the studied alloys. The Curie temperature, T_C, was calculated from the intersection of the steepest slope of the curve with the abscissa axis. In the case of *Co20Ge5* alloy, the decrease of M_S due to the ferro-paramagnetic transition of the amorphous phase slightly overlaps with the increase due to the formation of the α-Fe(Co,Ge) nanocrystals. The partial substitution of Co for Fe clearly increases T_C from 445 K (*Co0Ge0* alloy) up to ~520 K and up to >700 K for the alloys with 5 and 20 at. % of Co, respectively. However, partial substitution of Ge for B seems to have almost no effect on the Curie temperature (T_C slightly decreases from *Co5Ge0* alloy to *Co5Ge5* alloy), although partial substitution of Ge for Fe was proposed as a promising way for the enhancement of high temperature applications of nanocrystalline alloys [10]. However, it might be noticed that both B and Ge substitution for Fe increase the Curie temperature of amorphous Fe-B alloys [35]. Therefore, although partial substitution of Ge for Fe is effective for enhancing T_C of the amorphous phase for Fe-Zr-B-Cu alloys [10], the partial substitution of Ge for B is not. A direct measurement of the Curie temperature of the residual amorphous phase is only possible for a low nanocrystalline volume fraction. For the alloys with 5 at. % of Co a detailed studied was performed on the evolution of the Curie temperature with the annealing temperature and an increase of about 20-30 K was observed for both alloys after partial nanocrystallization [36].

From this point of view, although the partial substitution of Co for Fe is a good candidate to enhance the high temperature applications of nanocrystalline alloys, as it was shown for other nanocrystalline compositions [6,7,13], the partial substitution of Ge for B

seems to be ineffective. However, as it was demonstrated elsewhere [36], the nanocrystalline state formed in *Co5Ge5* alloy shows an enhancement of about 10 % of the saturation magnetization with respect to the *Co5Ge0* alloy. In general, for samples annealed up to the end of the nanocrystallization, this magnitude is larger for Ge-containing alloys (155-160 emu/g) than for Ge-free alloys (135-145 emu/g). In fact, the substitution of Ge for B in amorphous Fe-B alloys enhances the magnetic moment per Fe atom [35]. On the other hand, at high crystalline volume fractions, a strong enhancement of T_C^{AM} might be expected due to the polarizing effect of the ferromagnetic nanocrystals [37].

3.3.2 Coercivity

Room temperature coercivity values, H_C, were obtained for samples heated up to different temperatures, T_A. The evolution of H_C is closely related to the microstructural changes.

At temperatures below the onset of crystallization, H_C generally decreases due to the relaxation of the internal stresses, which provokes a decrease in the magnetoelastic anisotropy. However, the *Co20Ge5* alloy exhibits a totally opposed behavior and H_C increases as T_A increases below the onset temperature of crystallization. In this alloy, the annealing temperatures are lower than the Curie temperature of the amorphous system. Therefore, the increase of the temperature provokes a stabilization of the domain walls, which increases the coercivity of the material, as it was observed in other nanocrystalline systems [9].

A peak of the H_C values is detected in all the studied alloys at temperatures close to the observed onset of crystallization. At the early beginning of the nanocrystallization, isolated nanocrystals do not interact and, therefore, the magnetic anisotropy is not averaged out.

After this peak, an almost constant value of H_C is observed for each alloy. This value is ~40-50 A/m for the *Co20Ge5* alloy and ~10 A/m for the other alloys, values much lower

Acta Materialia. Vol. 53. Núm. 4. 2005. Pag. 1241-1251
http://dx.doi.org/10.1016/j.actamat.2004.11.018

than those obtained for alloys with a high Co concentration [6,9]. The higher values observed for the *Co20Ge5* alloy cannot be explained in terms of the microstructure (similar values of X and $<D>$ with respect to the other alloys, see fig. 3 and fig 4) but must be due to an increase of the magnetoelastic anisotropy due to a higher value of the magnetostriction. In fact, the saturation magnetostriction constant, λ_S, of α-Fe increases from –9 ppm, for pure Fe, to 30 ppm for a Co content of 20 at. % [38].

The values of λ_S were experimentally obtained using SAMR method for as-cast samples as 11, 15, 18 and 36 ppm for the *Co0Ge0*, *Co5Ge0*, *Co5Ge5* and *Co20Ge5* as-cast alloys, respectively. It can be observed that the partial substitution for Fe increases λ_S of the amorphous alloy, at least up to 20 at. % of Co content, in agreement with the observed trend for Fe-Co-B alloys [38]. The partial substitution of Ge for B also increases the value of λ_S for the amorphous samples. Unfortunately, the SAMR method could not be applied to nanocrystalline samples because they become very brittle after the thermal treatment. Nevertheless, it is possible to have an idea of the evolution of λ_S as the nanocrystallization progresses assuming a composition of the nanocrystals based on a homogeneous distribution of Co throughout the amorphous matrix and the crystalline phase [14,15] and neglecting the effect of the possible presence of Ge inside the nanocrystals. Therefore, the values of λ_S would be -9 ppm, for the *Co0Ge0* alloy, ~0 ppm, for both alloys with 5 % of Co, and ~30 ppm for the *Co20Ge5* alloy [38]. Thus, it can be easily understood that the magnetostriction value of the whole system, obtained as an average between the values of the crystals and the amorphous matrix, can be only cancelled out when λ_S of the α-Fe phase is negative, as it occurs for *Co0Ge0*. However, although a cancellation of the magnetostriction of the whole system is not possible when λ_S of the crystalline phase is positive, a reduction can be achieved if λ_S of the forming phase is smaller than the value of the amorphous phase, as it occurs for the alloys with 5 at. % of Co. Finally, if the value of λ_S of the crystalline phase is larger than

that of the amorphous system, an increase on the overall magnetostriction might be expected, as occurs for the *Co20Ge5* alloy.

After annealing at higher temperatures, a severe hardening is observed for all the studied alloys up to 6-7 kA/m, which corresponds to the formation of intermetallic (Zr and B containing) phases. The formation of these phases marks an irreversible temperature limit for the application of these alloys as soft magnets.

4. Conclusions

From the present study, several conclusions can be drawn:

- The partial Co substitution for Fe decreases the thermal stability of the as-cast amorphous system. The partial substitution of Ge for B also produces the same effect and strongly affects the melting process of the alloy. The kinetic parameters of the first crystallization stage (Q = 3-4 eV, n~1) are typical for nanocrystallization processes.
- The position of the amorphous halo in the XRD pattern shifts to lower values of 2θ as the nanocrystallization progresses even if a high enrichment of B in the amorphous matrix is expected. This should indicate that this parameter is mainly related with the average distance between neighbor metallic atoms, due to the low scattering power of B atoms.
- During the first crystallization stage, a similar nanocrystalline microstructure is developed for all the studied alloys (<D>~10 nm and a maximum X~0.80-0.85). Ge substitution increases a with respect to the Ge-free alloys, indicating the presence of some Ge content in the nanocrystals, although lower than the average concentration in the alloy. A continuous decrease of a as the nanocrystallization progresses is observed even for samples with an expected pure Fe composition of the crystalline phase. The lattice dilatation could be an effect of the very small grain size, as it was observed for other nanocrystalline systems.

Acta Materialia. Vol. 53. Núm. 4. 2005. Pag. 1241-1251
http://dx.doi.org/10.1016/j.actamat.2004.11.018

- The XRD patterns of fully crystallized samples are more complex for Ge-containing alloys, for which an extra Zr-rich phase appears. The $Fe_{23}Zr_6$ phase has been detected for the *Co20Ge5* alloy but not for the other alloys.
- Partial Co substitution for Fe is clearly efficient for enhancing the Curie temperature of the amorphous phase, although Ge substitution for B seems to have no effect on T_C^{AM}. However, Ge-containing alloys have a higher saturation magnetization for samples annealed up to the end of the nanocrystallization.
- The coercivity of nanocrystalline samples is clearly larger for the *Co20Ge5* alloy than for the other studied alloys, which is due to the higher magnetostriction of the two phases present in the nanocrystalline microstructure.

Finally, the *Co5Ge5* alloy can be considered the optimum composition among the studied alloys in this work. The Curie temperature of the initial amorphous phase is enhanced only by ~70 K with respect to the Co- and Ge-free alloy. However, the nanocrystalline microstructure achieved is stable up to ~1000 K and the soft magnetic properties are characterized by a high M_S ~150 emu/g (~1.4 T) and a low coercivity at room temperature H_C ~10 A/m.

Acknowledgments

This work was partially supported by the Spanish Government and EU FEDER (Project MAT 2001-3175). J.S. Blázquez acknowledges a research contract from the Regional Government of Andalucía (Spain).

Acta Materialia. Vol. 53. Núm. 4. 2005. Pag. 1241-1251
http://dx.doi.org/10.1016/j.actamat.2004.11.018

References

[1] McHenry ME, Willard MA, Laughlin DE. Progress in Mater Sci 1999; 44: 291

[2] Herzer G. IEEE Trans Magn 1989; 25: 3327

[3] Hernando A, Vázquez M, Kulik T, Prados C, Phys. Rev. B 1995; 51: 3581

[4] Suzuki K, Makino A, Kataoka N, Inoue A, Masumoto T. Mater Trans JIM 1991; 32: 93

[5] Suzuki K, Makino A, Inoue A, Masumoto T. J Appl Phys 1991; 70: 6232

[6] Willard MA, Laughlin DE, McHenry ME, Thoma D, Sickafus K, Cross JO, Harris VG. J Appl Phys 1998; 84: 6773

[7] Müller M, Grahl H, Mattern N, Kühn U, Schnell B. J. Magn. Magn. Mat. 1996; 160**:** 284

[8] Blázquez JS, Franco V, Conde A, Kiss LF. J Appl Phys 2003; 93: 2172

[9] Blázquez JS, Franco V, Conde A, Gibbs MRJ, Davies HA, Wang ZC. J Magn Magn Mat 2002; 250: 260

[10] Suzuki K, Cochrane JW, Cadogan JM, Xiong XY, Hono K. J Appl Phys 2002; 91: 8417

[11] Cremaschi V, Saad A, Moya J, Arcondo B, Sirkin H. Physica B 2002; 320: 281

[12] Narita K, Yamasaki J, Fukunaga H. IEEE Trans Magn 1980; 16: 435

[13] Blázquez JS, Conde CF, Conde A. J Non-Cryst Solids 2001; 287: 187

[14] Ping DH, Wu YQ, Hono K, Willard MA, McHenry ME, Laughlin DE. Scripta Mater 2001; 45: 781

[15] Zhang Y, Blázquez JS, Conde A, Warren PJ, Cerezo A. Mater Sci Eng A 2003; 353: 158

[16] Jedryka E, Wójcik M, Svec P, Skorvanek I. Appl Phys Letters 2004; 85:2884

[17] Kissinger HE. Anal Chem 1957; 29: 1702

[18] Augis JA, Bennett JE. J Thermal Anal 1978; 13: 283

[19] Gao YQ, Wang W. J Non-Cryst Solids 1986; 81: 129

[20] Yinnon H, Uhlmann DR. J Non-Cryst Solids 1983; 54: 253

[21] Altúzar P., Valenzuela R. Mat Letters 1991; 11: 101

[22] McHenry ME, Johnson F, Okumura H, Ohkubo T, Ramanan VRV, Laughlin DE, Scripta Mater 2003; 48: 881

[23] Hsiao A, McHenry ME, Laughlin DE, Kramer MJ, Ashe C, Ohkubo T, IEEE Trans Magn 2002; 38: 3039

[24] Blázquez JS, Conde CF, Conde A, Appl Phys A 2003; 76: 571

[25] Massalski TB, Okamoto H, Subramanian PR, Kacprzak L. Binary Alloys Phase Diagrams. Materials Park, Ohio: ASM International, 1992. p. 1187, 1706.

[26] Egami T. In: Liebermann HH, editor. Rapidly Solidified Alloys: Processes, Structures, Properties, Applications. New York: Marcel Dekker, INC. p. 232.

[27] Smithells CJ. Metals Reference Book, vol. 1. London: Butterworths, 1967. p. 100.

[28] Cullity BD. Elements of X-ray Diffraction. Reading: Addison-Wesley, 1956. p. 474.

[29] Zhao YH, Zhang K, Lu K. Phys. Rev. B 1997; 56: 14322

[30] Bozorth RM. Ferromagnetism. Princeton (NJ): Van Nostrand, 1968. p. 192.

[31] Pearson WB. A Handbook of Lattice Spacings and Structures of Metals and Alloys, vol. 2. Oxford: Pergamon Press, 1967. p. 911.

[32] de Boer FR, Boom R, Mattens WCM, Miedema AR, Niessen AK. Cohesion in Metals. Transition Metal Alloys. Amsterdam: North-Holland, 1989. p. 233, 276, 375.

[33] Zhu DM, Raviprasad K, Suzuki K, Ringer SP. J Phys D: Appl Phys 2004; 37: 645

[34] Blázquez JS, Conde CF, Conde A. Appl Phys Letters 2001; 79: 2898

[35] Wijn HPJ. Landolt-Börnstein: Magnetische Eigenschaften von Metallen, vol. 19. Berlin: Springer Verlag, 1991. p. 93, 104.

[36] Blázquez JS, Roth S, Conde A, in preparation

[37] Hernando A, Navarro I, Prados C, García D, Lesmes F, Freijo JJ, Salcedo A. Nanostruct Mater 1997; 9: 459

[38] O'Handley RC. Modern Magnetic Materials: Principles and Applications. New York: Wiley, 1999. p. 227.

Acta Materialia. Vol. 53. Núm. 4. 2005. Pag. 1241-1251
http://dx.doi.org/10.1016/j.actamat.2004.11.018

Figure captions

Figure 1. DSC scans of as-cast samples of all studied alloys obtained at 20 K/min: T_{p1}, T_{p2} and α-γ indicate the temperature of the first and the second crystallization processes and the allotropic transition from α-Fe to γ-Fe, respectively. The deviation of the DSC signal above 1250 K is an artifact due to the baseline.

Figure 2. 2θ position of the amorphous halo, $x_C^{AM}(2\theta)$, after deconvoluting from the (110) maximum of α-Fe against annealing temperature (a) and average distance between atoms, δ, as a function of crystalline fraction (b) obtained from the 2θ position of the halo (squares) and calculated as the average diameter of all the atoms in the residual amorphous matrix (triangles) and excluding B from this averaging (crosses).

Figure 3. Crystalline volume fraction, X, as a function of the difference between the annealing temperature and the onset of nanocrystallization, T_A-T_X.

Figure 4. Average grain size, $\langle D \rangle$, (a) and lattice parameter, a, (b) against the crystalline volume fraction of α-Fe nanocrystals.

Figure 5. TEM bright field images and corresponding selected area diffraction patterns (inset) for samples of *Co5Ge5* (up) and *Co20Ge5* (down) heated up to 873 K.

Figure 6. XRD patterns of samples heated up to 1073 K (fully crystallized samples). (o) α-Fe, (×) diffraction maxima appearing for Ge-free alloys, (+) new maximum appearing for Ge-containing alloys (Zr-rich phase) and (|) $Fe_{23}Zr_6$ phase.

Figure 7. Saturation magnetization, M_S, versus temperature for as-cast alloys. The arrows indicate the Curie temperatures.

Acta Materialia. Vol. 53. Núm. 4. 2005. Pag. 1241-1251
http://dx.doi.org/10.1016/j.actamat.2004.11.018

Table I. Relevant parameters of the devitrification and melting process of the alloys obtained at a heating rate $\beta = 20$ K/min. T_X, crystallization onset temperature; T_{Pi}, peak temperature of the i^{th} process; ΔH_i, enthalpy of transformation of the i^{th} process; T_m, onset temperature of the melting.

Alloy	T_X ± 2 K	T_{P1} ± 1 K	ΔH_1 ± 5 %	T_{P2} ± 1 K	ΔH_2 ± 5 %	T_m ± 10 K
$Fe_{83}Zr_6B_{10}Cu_1$	783	807	71	1002	36	1270
$Fe_{78}Co_5Zr_6B_{10}Cu_1$	773	796	73	997	38	1260
$Fe_{78}Co_5Zr_6B_5Ge_5Cu_1$	758	779	73	1007	37	1220
$Fe_{63}Co_{20}Zr_6B_5Ge_5Cu_1$	737	757	80	1000	37	1185

Acta Materialia. Vol. 53. Núm. 4. 2005. Pag. 1241-1251
http://dx.doi.org/10.1016/j.actamat.2004.11.018

Table II. Kinetic parameters of the nanocrystallization process obtained by non-isothermal approximations.

Alloy	*Q* (± 0.2 eV)			*n* (± 0.2)
	Kissinger	*Gao-Wang*	*Augis-Bennett*	*Gao-Wang*
$Fe_{83}Zr_6B_{10}Cu_1$	3.9	4.1	4.3	1.2
$Fe_{78}Co_5Zr_6B_{10}Cu_1$	3.6	3.7	4.1	1.0
$Fe_{78}Co_5Zr_6B_5Ge_5Cu_1$	3.2	3.3	3.4	1.0
$Fe_{63}Co_{20}Zr_6B_5Ge_5Cu_1$	2.8	2.9	3.2	0.9

Acta Materialia. Vol. 53. Núm. 4. 2005. Pag. 1241-1251
http://dx.doi.org/10.1016/j.actamat.2004.11.018

Figure 1

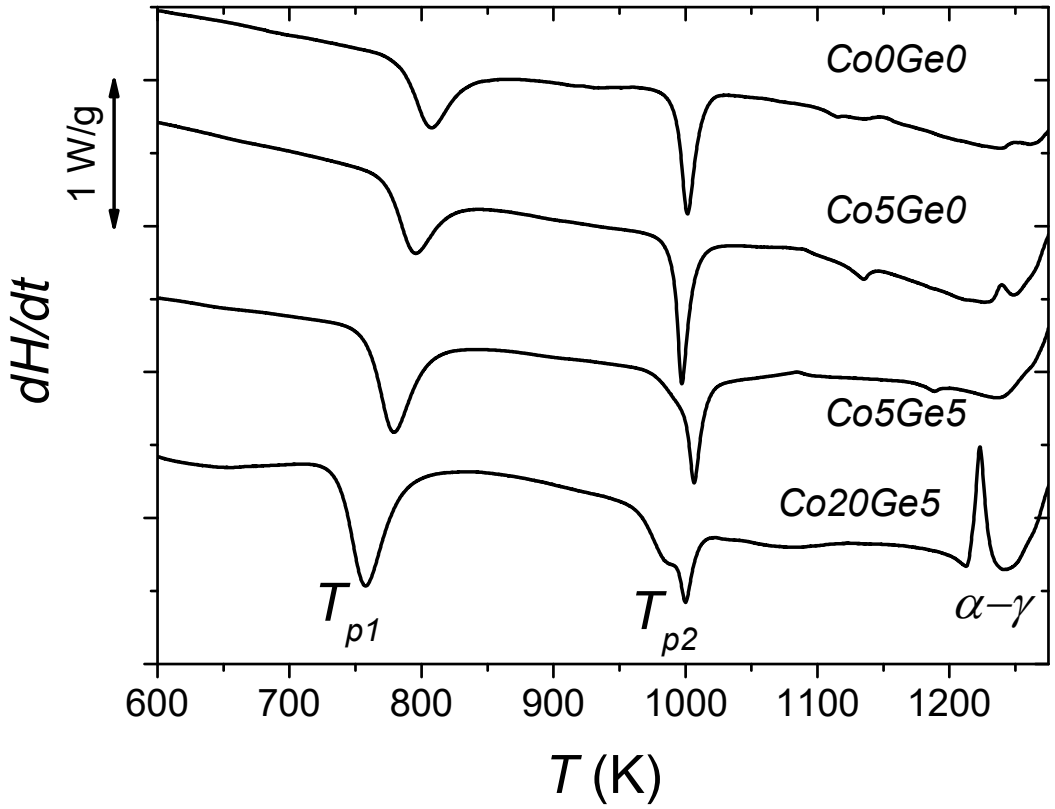

Acta Materialia. Vol. 53. Núm. 4. 2005. Pag. 1241-1251
http://dx.doi.org/10.1016/j.actamat.2004.11.018

Figure 2

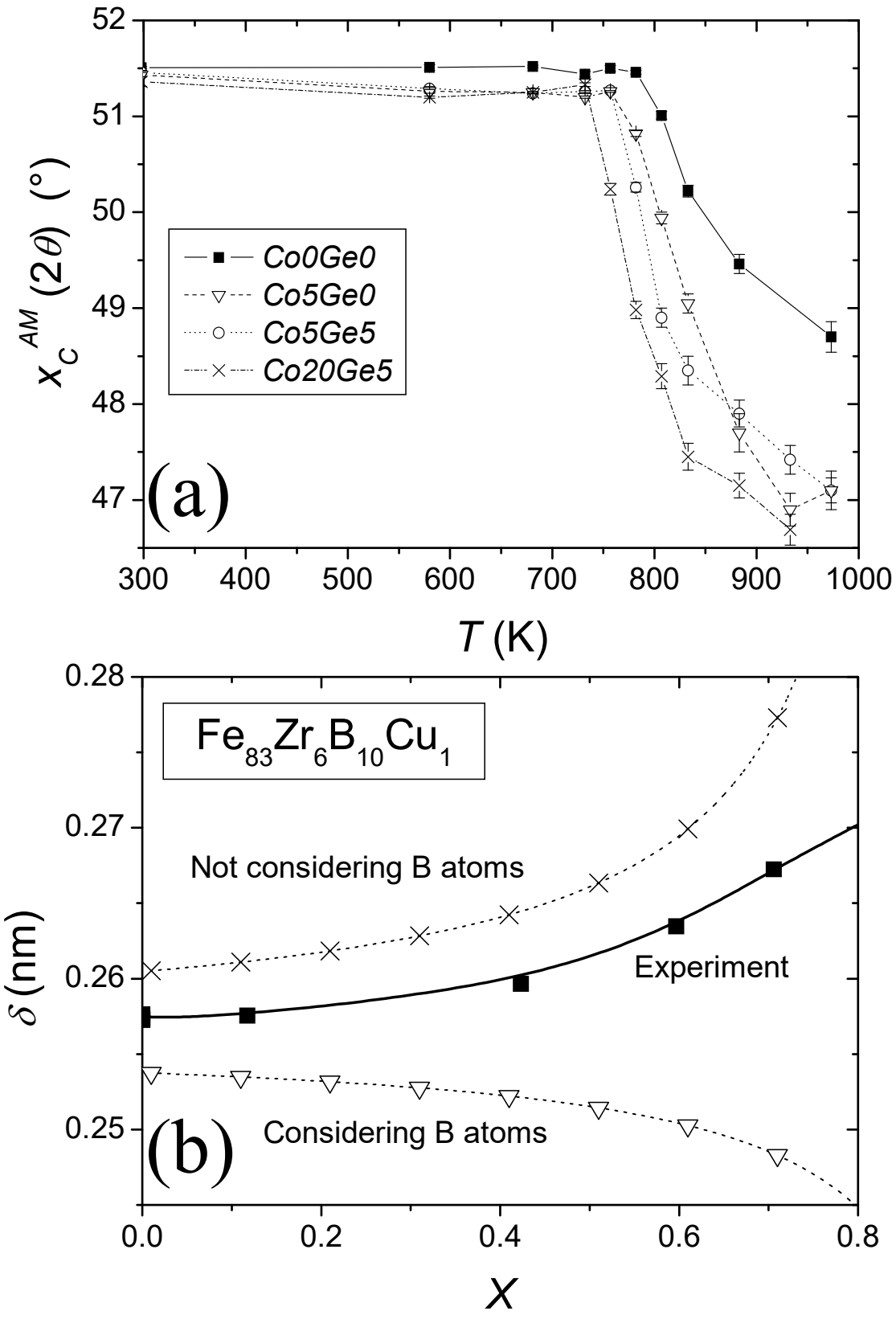

Acta Materialia. Vol. 53. Núm. 4. 2005. Pag. 1241-1251
http://dx.doi.org/10.1016/j.actamat.2004.11.018

Figure 3

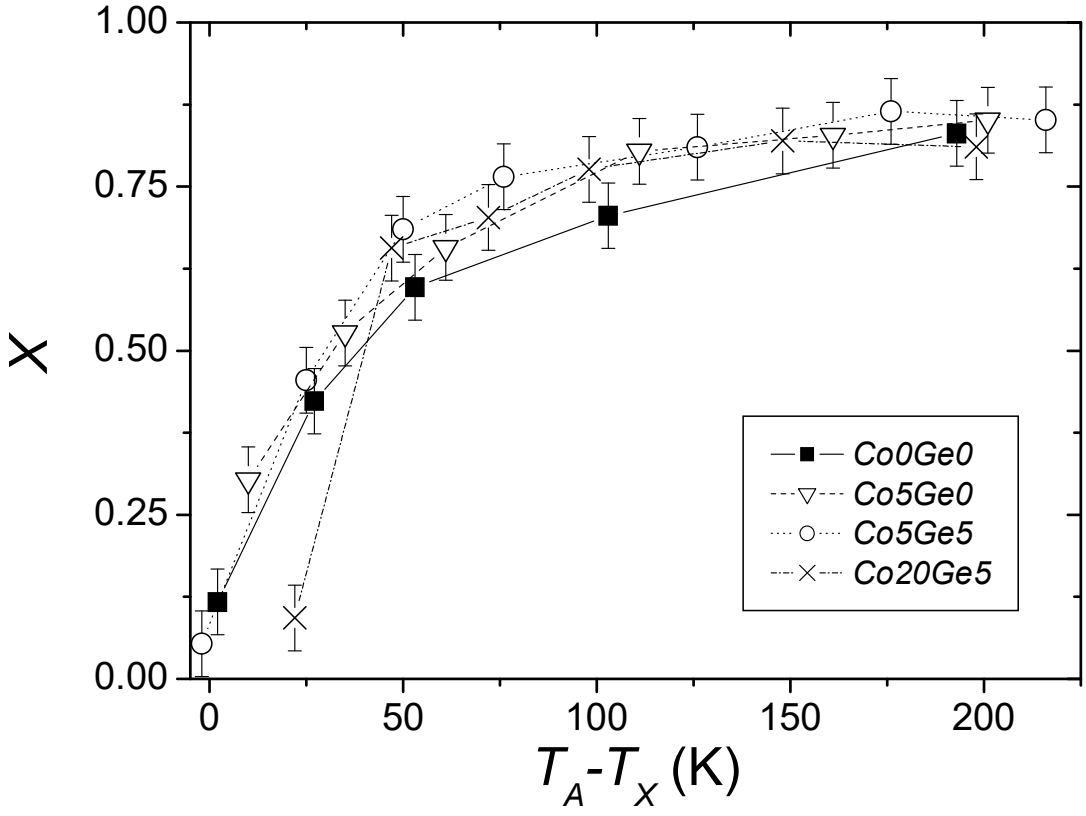

Acta Materialia. Vol. 53. Núm. 4. 2005. Pag. 1241-1251
http://dx.doi.org/10.1016/j.actamat.2004.11.018

Figure 4

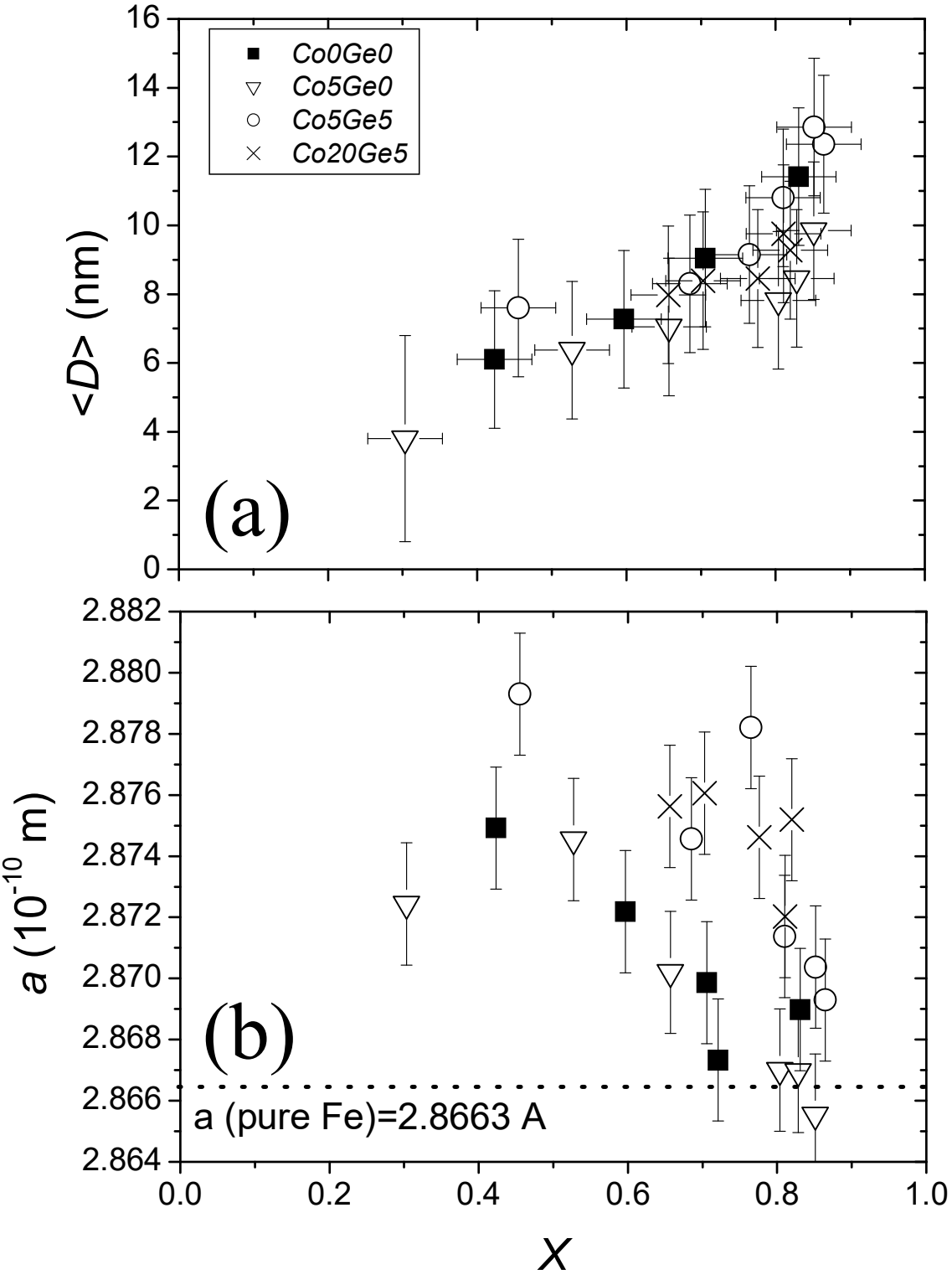

Acta Materialia. Vol. 53. Núm. 4. 2005. Pag. 1241-1251
http://dx.doi.org/10.1016/j.actamat.2004.11.018

Figure 5

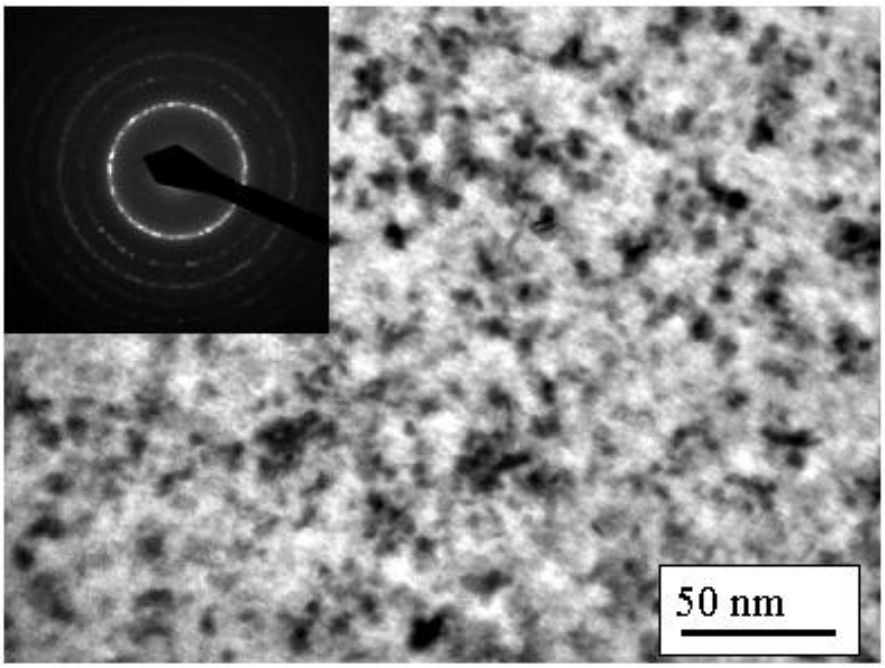

Co5Ge5; T_A=823 K

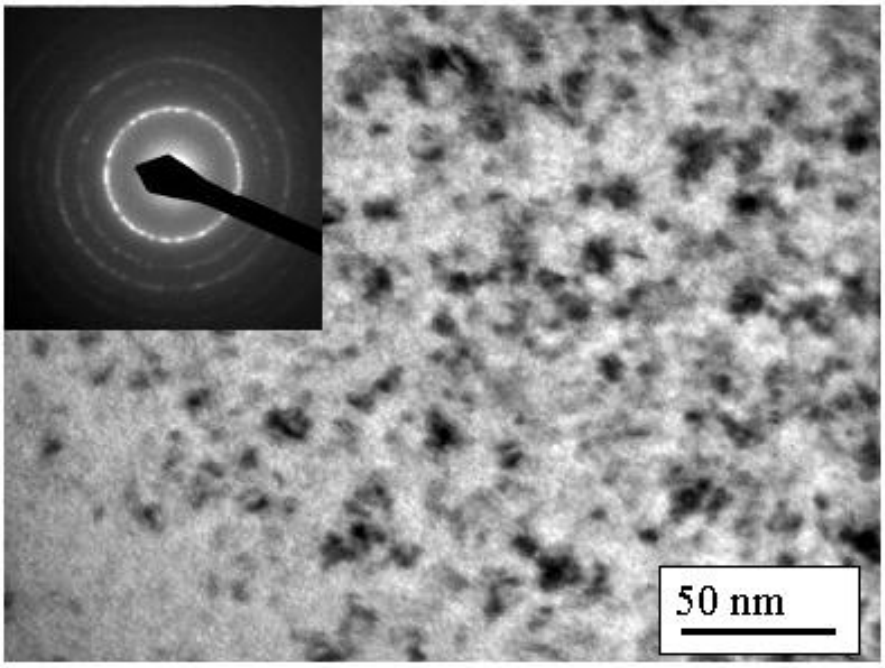

Co20Ge5; T_A=823 K

Acta Materialia. Vol. 53. Núm. 4. 2005. Pag. 1241-1251
http://dx.doi.org/10.1016/j.actamat.2004.11.018

Figure 6

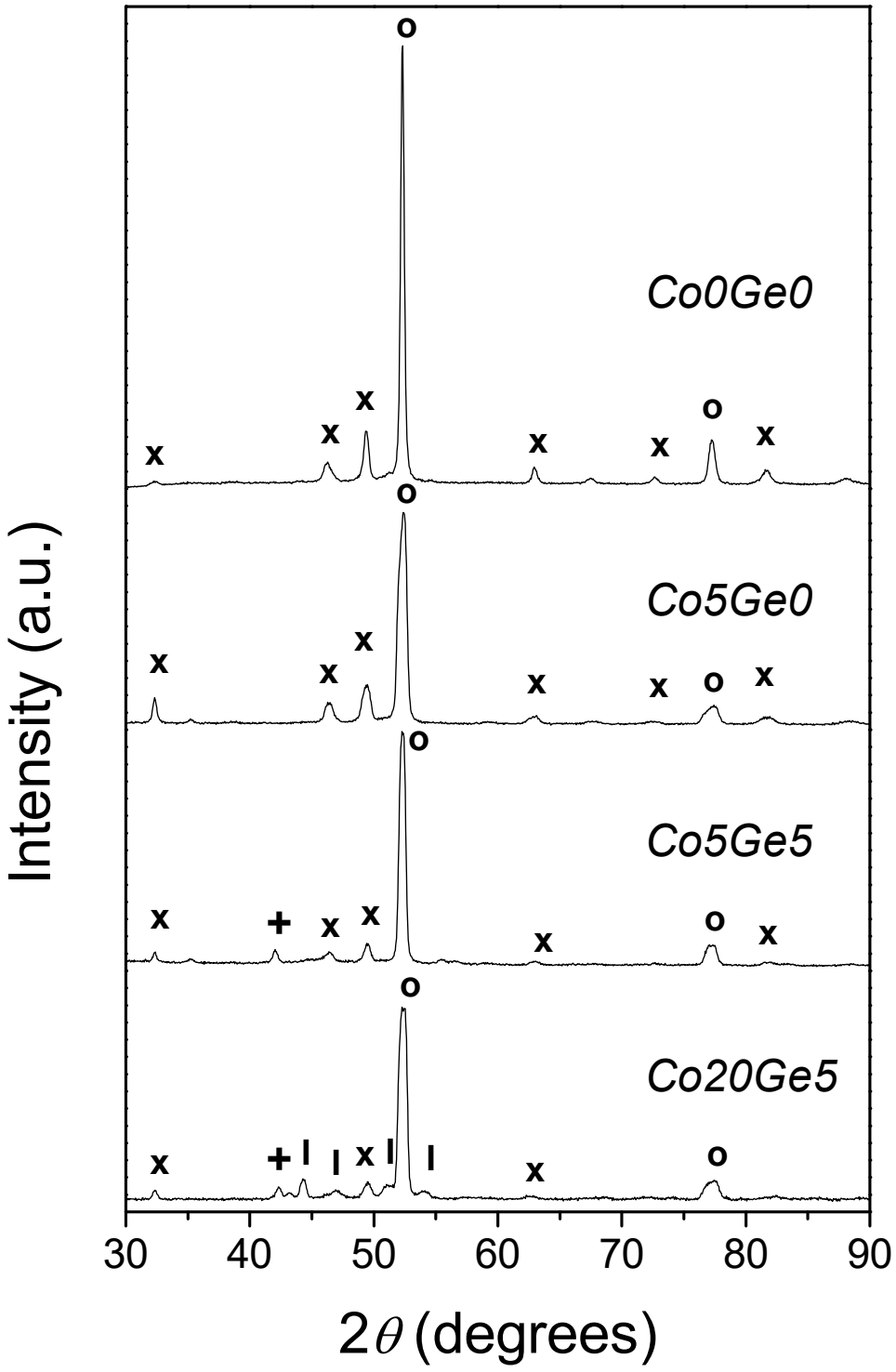

Acta Materialia. Vol. 53. Núm. 4. 2005. Pag. 1241-1251
http://dx.doi.org/10.1016/j.actamat.2004.11.018

Figure 7